JOURNAL OF COMPUTATIONAL BIOLOGY
Volume 25, Number 11, 2018

Pp. 1231–1246
DOI: 10.1089/cmb.2017.0131

Probabilistic Modeling of Pseudorabies Virus Infection in a Neural Circuit

SIAMAK K. SOROOSHYARI,[1] MATTHEW P. TAYLOR,[2] and H. VINCENT POOR[3]

ABSTRACT

Viral transneuronal tracing methods effectively label synaptically connected neurons in a time-dependent manner. However, the modeling of viral vectors has been largely absent. An objective of this article is to motivate and initiate a basis for computational modeling of viral labeling and the questions that can be investigated through modeling of pseudorabies virus (PRV) virion progression in a neural circuit. In particular, a mathematical model is developed for quantitative analysis of PRV infection. Probability expressions are presented to evaluate the progression of viral labeling along the neural circuit. The analysis brings forth various parameters, the numerical values of which must be attained through future experiments. This is the first computational model for PRV viral labeling of a neural circuit.

Keywords: probabilistic modeling, pseudorabies virus, viral tracing.

1. INTRODUCTION

Vertebrate nervous systems are collections of specialized cells termed neurons. Neurons transmit information through a combination of electrical and chemical signals that propagate between neurons at points of contact termed synapses. Neurons function by forming many connections to transmit a wide array of information. These connections link neurons together into circuits. A goal of modern neuroanatomy is to define the circuits that correlate with brain function and processing. The use of viral tracers to define the organization of projection pathways of neurons has proven to be integral to mapping the functional organization of the nervous system. Classical approaches to define projection patterns of neurons exploit vesicular transport. Such staples of circuit analysis include molecules that are taken up by axons and transported back to the cell soma (retrograde labeling), or are incorporated into neuronal somata and transported through axons to label axonal terminal fields (anterograde labeling). The extensive application of such tracers has produced a massive database establishing regional associations among distributed populations of neurons.

However, the inability of these molecules to cross synapses has hindered efforts to define systems that function collectively through their synaptic connections to accomplish specific functions. The introduction of viruses for circuit analysis has filled this void. Neurotropic viruses can cause widespread pathology in the nervous system by virtue of their ability to spread through neural circuitry. Neuroanatomists in collaboration with virologists have exploited this ability to define polysynaptic connections in the brain. The success of this approach has emerged from concerted efforts to identify strains of virus with reduced

[1]Johnson & Johnson, Bridgewater, New Jersey.
[2]Department of Microbiology and Immunology, Montana State University, Bozeman, Montana.
[3]Department of Electrical Engineering, Princeton University, Princeton, New Jersey.

virulence that retain the ability to infect and spread within neural circuitry. A concise description of the importance of viral trafficking in neurons is provided in Enquist (2012). Viral tracing of neural circuitry has become a powerful tool for neuroscientists with its advancement benefiting numerous contemporary neuroscience research projects. The ability of neurotropic viruses to replicate and pass through synaptic connections has provided a polysynaptic perspective on the organization of a variety of neural circuits.

The Bartha strain of pseudorabies virus (PRV), a swine alpha herpesvirus, was identified on the basis of these features, and is extensively used for circuit analysis. Bartha was originally developed as a vaccine strain, and subsequent analysis identified deletions and mutations in the viral genome causal for the reduction in virulence. Proof of principle through such studies has led to the widespread use of Bartha for circuit definition, and has also stimulated the production of Bartha recombinants that constitutively or conditionally express reporters that facilitate neuronal labeling. Mechanistic studies have demonstrated that transneuronal transport of Bartha restricts labeling to the retrograde direction between synaptically connected neurons.

Recombinant viruses with well-documented deletions and mutations have proven to be important in defining the mechanisms of viral spread that contribute to viral disease. The comprehension of viral trafficking and its effects within a neural circuit will provide fundamental knowledge toward the development of methods to block neuronal invasion and spread, as well as provide insight into neural circuit organization. This work introduces a three-stage model for the propagation of PRV in a neural circuit consisting of multiple neurons. Stage 1 models the capacity for viral particles to engage in receptor-mediated infection of axons. Stage 2 models the establishment of infection and transmission of infectious virus across synaptic contacts. Stage 3 models the progression of infection between synaptically connected neurons, which results in second-order infection (SOI) and subsequent higher order infection (HOI). Our attention is restricted to PRV Bartha due to its popularity and utility for transneuronal tracing. More specifically, PRV Bartha and its recombinants infect synaptically connected circuits through retrograde transneuronal passage, either through peripherally projecting axons of somatic and autonomic neurons or after direct injection into the brain.

2. MODEL FORMULATION

An impetus for this work was provided through a figure in Card and Enquist (2012) reproduced herein and referred to as the model neural circuit for studying viral uptake with axonal transport capabilities. The neural circuit model in Figure 1 illustrates the virus replicating at a primary neuron, proceeding through retrograde transmission to infect a secondary neuron in synaptic contact, and subsequently maturing as a HOI. We shall analytically model the likelihood of a HOI occurring by considering how the most crucial variables in Figure 1 can influence the progression of the infection through a circuit. Figures 1–3 present a tantamount representation of the neural circuit and will facilitate the probabilistic modeling of infectious viral spread. It is the goal of this work to present a first-principles approach for the quantitative depiction of such a complex process. The three-stage scheme introduced in Figures 2 and 3 shall be expanded upon and referenced throughout this work. The presented model will be based upon a tissue architecture dominated by a high density of axons (Card et al., 1999).

The mathematically oriented analysis in this work will be of greater practical value if the results are eventually validated by experimental data. The experimental paradigm of stereotactic injection of virus into the rat striatum can test the predictive capabilities of the presented analysis. As in our analysis, the rat striatum has a tissue architecture with high axon density and defined synaptic contacts for HOI. In addition, the outcome of the mathematical model can be applied to other experimental paradigms and provide additional interpretation of many neuroanatomical tracing studies. The focus of this mathematical framework is the analysis of virion uptake, and transmission between primary and secondary neurons. We believe that directing our analysis at a system with a larger depth of knowledge will enhance the model formulation. New studies are being performed with multiple viruses to differentially label neurons based on the directional spread of infection. As more studies are published, their findings will continue to inform our mathematical models of PRV neuroinvasion.

3. STAGE 1: AXONAL INVASION

It is assumed that 1 million PRV particles (i.e., virions) are injected and exposed to axon terminals at the injection site. PRV entry requires specific receptors, and we shall assume a uniform distribution of the

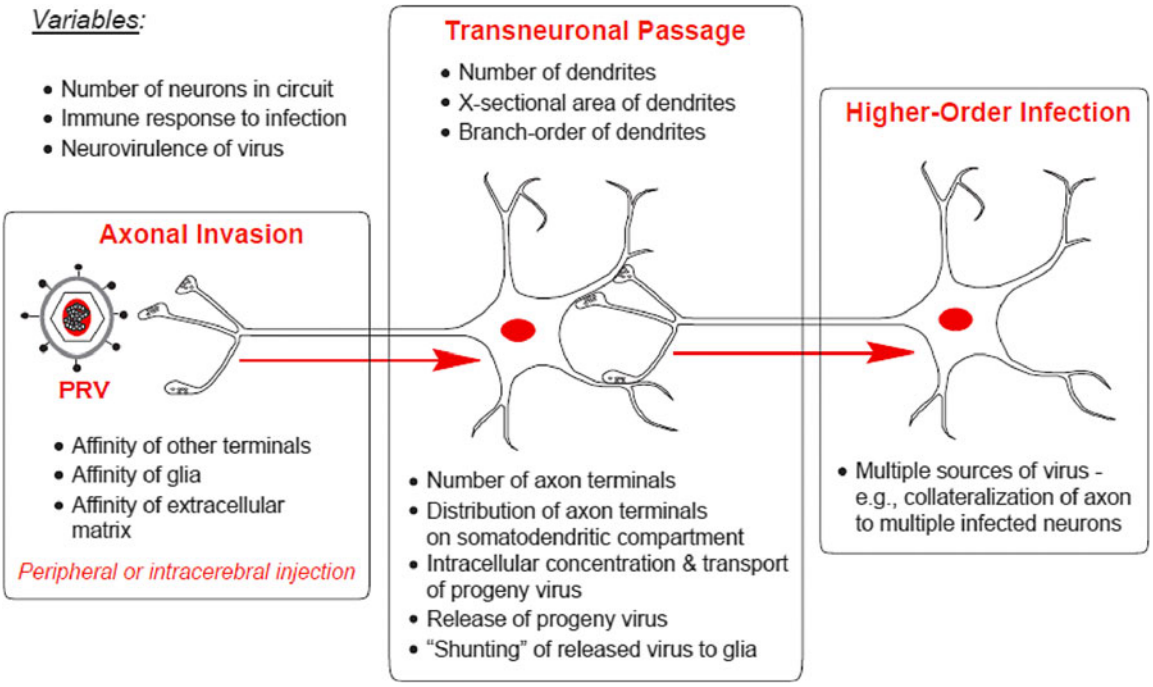

FIG. 1. A depiction of retrograde PRV progression along three stages in a neural circuit as advocated in Card and Enquist (2012). PRV, pseudorabies virus.

receptors on all axon terminals. PRV virions are large (~ 200 nm in diameter), and their movement by diffusion in the extracellular space is rather limited. Also, interactions of the membrane proteins on the virion envelope with extracellular matrix proteins such as heparan sulfate proteoglycan further limit the extent of extracellular movement.

3.1. Parameters associated with receptor-mediated infection

The ith receptor will mediate an infection with a probability denoted by $P[R_i = I]$, where $i = 1, 2, \ldots, R$. We propose the following relationship:

$$P[R_i = I] = W(\alpha_i e^{-d_i/\bar{d}} + \beta_i + \gamma_i + \omega_i), \tag{1}$$

where d_i represents the distance from the ith receptor to the point of injection and $\bar{d}$ denotes the mean receptor distance to the point of injection for the close vicinity surrounding the injection area.

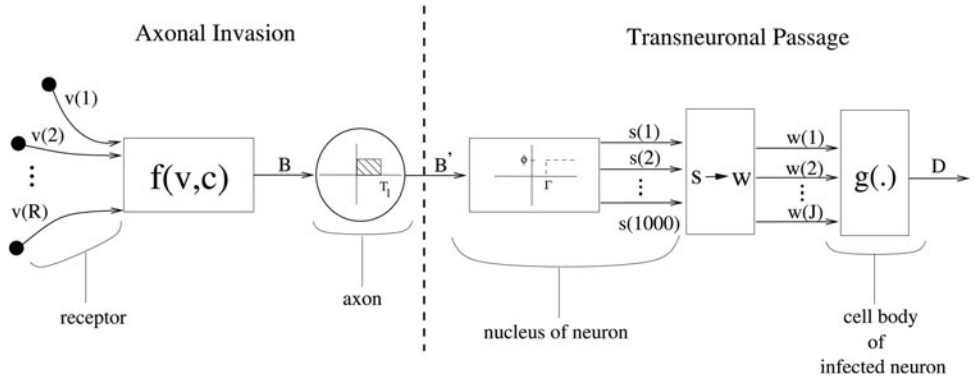

FIG. 2. An analytical model of PRV progression along the first two stages—axonal invasion and transneuronal passage—of a neural circuit with a single axon and a single neuron.

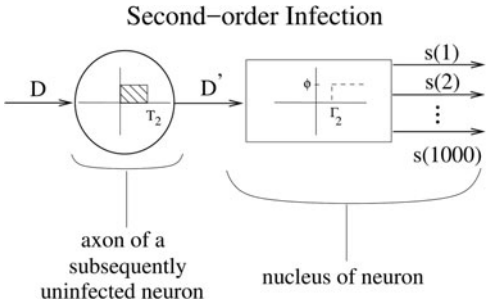

FIG. 3. A model for PRV progression along the HOI stage of a neural circuit. The second-order neuron is depicted with a single axon connecting it to the transneuronal passage stage of a first-order neuron. HOI, higher order infection.

The five parameters that affect the likelihood of the i th receptor mediating an infection are described as follows:

- α_i represents the contribution of the proximity of the receptor to the point of injection,
- β_i denotes the contribution of the affinity of the axon terminal,
- γ_i expresses the contribution of the affinity of glia,
- ω_i represents the contribution of the affinity of extracellular matrix, and
- W describes the anatomical impact on the likelihood of infection.

We specify $0 \leq \alpha_i + \beta_i + \gamma_i + \omega_i \leq 1$ with $\alpha_i, \beta_i, \gamma_i, \omega_i \in [0, 1]$ as free parameters, which must be determined empirically. The aforementioned inequality for the sum of the four free parameters must be obeyed to assure that Equation (1) is a probability. The precise quantitative relationship between α_i, β_i, γ_i, ω_i, and $P[R_i = I]$ is not precisely known with Equation (1) being a proposition. An important receptor for PRV in rodent neurons is nectin 1, a cellular adhesion molecule (Takai and Nakanishi, 2003). The efficiency of binding of PRV virions to nectin 1 in tissue for the ith receptor has been modeled in Equation (1) through the parameter β_i. It has been empirically determined in works, such as Card et al. (1999), that the affinity of axon terminals dominates two of the aforementioned variables as far as influence on the likelihood of a receptor mediating infection, in other words, $\beta_i \gg \gamma_i$ and $\beta_i \gg \omega_i$. In light of this discussion, we posit that the probability of receptor-mediated infection can be approximated as

$$P[R_i = I] \approx W(\alpha_i e^{-d_i/\bar{d}} + \beta_i), \tag{2}$$

which also serves as a good approximation to Equation (1) for the case of the rat striatum (Card et al., 1999). It is important to note that affinity within the context of the above parameters refers to the strength of coupling between viral glycoproteins and the nectin adhesion molecule. The outcome of the prospective interactions would lead to the fusion of the virion envelope with the plasma membrane of the target cell, or result in binding the virion to the extracellular matrix.

The parameter $W \in [0, 1]$ in Equations (1) and (2) reflects the likelihood of infection based on the anatomical region that is injected. A scenario of $W \approx 0$ indicates that receptor-mediated infection will occur with very low likelihood; while $W = 1$ indicates that an infection will occur with high likelihood. An example of $W \approx 1$ is injection to the kidney. The kidney is a parenchymal organ with low extracellular fluid volume and high packing density of cells permissive to infection. The fact that the axonal plexus is sparse within this tissue (at least compared with axonal density within the brain) is not particularly relevant since the kidney cells will become infected and produce infectious progeny that will amplify the amount of infected virus. Thus, even if an axon terminal is not infected by the initial inoculum it is likely to be infected by the progeny virus produced by the kidney. Conversely, an example of $W \approx 0$ is injection to the spleen. The open circulation of the vasculature in the spleen immediately dilutes (and removes) virions from the site of injection to reduce the likelihood of local infection compared with the kidney. This is supported by the need to inject much higher quantities of virus into the spleen to achieve a productive infection of the neuronal innervation.

Thus, to obtain infections of kidney circuits, a viral injection containing only a fraction of the concentration of virus necessary to infect spleen circuits will be sufficient (Cano et al., 2001; Cano et al., 2004). In the case of the rat striatum, it was shown in Card et al. (1999) that the zone of viral uptake was confined

to a maximum radius within the range $0 \leq \max\{d_i\} \leq 1500\mu m$ of the cannula after injection of 100 nL of the highest concentration of virus. Very similar empirical findings were reported in Jasmin et al. (1997). A sensible choice for the mean of this parameter would be $E[\max\{d_i\}] = 500\mu m$.

Although values for several of the parameters that determine $P[R_i = I]$ have been discussed above, unfortunately, at the present time no empirical data exist for the probability of receptor-mediated infection. A viral reporter protein can be used to categorize a cell body as infected/noninfected once viral capsids are transported within axons to the cell body. However, it is practically impossible to have a complete tally of the total number of uninfected receptors. While the empirical determination of $P[R_i = I]$ may not be possible at the present time, the above analysis has discussed a means for analytical estimation of the probability of receptor-mediated infection by analytically stating its most prominent factors. For instance, Equation (2) implies the importance of performing experiments to determine a function (which may be obtained through a regression analysis) that maps nectin, or the properties of nectin, to the quantity β_i for a specific receptor.

3.2. Statistical modeling of receptor-mediated infection

The number of virions in the injected volume that bind to receptors is a random variable. It is suspected that many of the particles are simply bound to the extracellular matrix and do not bind to a receptor (Spear, 1993; Trybala et al., 1998; Pomeranz et al., 2005). The amount of particles that overcome the intrinsic host barriers to infection depends crucially on where an injection is made (e.g., into a muscle, a visceral organ, or the brain). We consider R receptors and define the R-dimensional vector $\mathbf{v}$ with its components having a Bernoulli distribution, where $\mathbf{v}(i)$ denotes whether the ith receptor mediates an infection ($\mathbf{v}(i) = 1$) or not ($\mathbf{v}(i) = 0$). Consequently, a random variable r will have the following physical interpretation $r = \sum_{i=1}^{R} \mathbf{v}(i)$ and a binomial distribution. An important variable of the axonal invasion stage shown in Figure 2 is quantified through

$$B = f(\mathbf{v}, \mathbf{c}) = \mathbf{v}^T \mathbf{c}, \tag{3}$$

where B represents the number of entered capsids. The vector $\mathbf{c} \in \mathbb{R}^R$ in Equation (3) represents weights that model the superposition of the viral capsids present on the R receptors at the beginning of an axon, while the process of retrograde transport to the neuronal cell body takes place. Equation (3) subsumes a linearized model for the combining. Unfortunately, in vivo data do not exist for the quantity B discussed above, and the empirical methods using in vitro studies have not been deemed relevant because of the inability to satisfactorily model the environment of the neuropil. Accordingly, attainment of experimental data for B is an avenue that we would like to motivate.

Despite the paucity of empirical data for a crucial parameter, analytical modeling can yield headway and insight into the progression of the viral tracer. For instance, the assumption of a homogeneous likelihood for receptor-mediated infection through $P[R_i = I] = P[R = I] = P$ allows for a preliminary analysis of the number of entered capsids B as a function of the likelihood of receptor-mediated infection. Such a scenario yields the discrete probability distribution:

$$P[B = b \,|\, \mathbf{c}] = P\left[\mathbf{v}^T \mathbf{c} = b \,|\, \mathbf{c}\right] = \begin{cases} P^R & b = \sum_{i=1}^{R} \mathbf{c}(i) \\ P(1-P)^{R-1} & b \in S_1 \\ P^2(1-P)^{R-2} & b \in S_2 \\ \vdots & \vdots \\ P^j(1-P)^{R-j} & b \in S_j \\ \vdots & \vdots \\ P^{R-1}(1-P) & b \in S_{R-1} \\ (1-P)^R & b = 0 \\ 0 & \text{otherwise} \end{cases}, \tag{4}$$

where we have conditioned on the vector $\mathbf{c}$, j denotes the number of receptor-mediated infections, and S_j denotes the set of all possible sums of j $\mathbf{c}(i)$ terms. For example, the set $S_3 = \{\mathbf{c}(a) + \mathbf{c}(b) + \mathbf{c}(c) : a \neq b \neq c\}$ will have $R(R-1)(R-2)$ elements accounting for all of the sums of possible combinations of three tuples. Unfortunately, empirical data on the distribution of the weights $\mathbf{c}(i)$ are also lacking. It is logical to presume

that $\mathbf{c}(i) \geq 0$ since a combination of infections cannot decrease the likelihood of capsids entering an axon terminal. The case of $\mathbf{c}(i) = 1 \; \forall i$ leads to B having a binomial distribution given by

$$P[B=b] = \binom{R}{b} P^b (1-P)^{R-b} \qquad \text{for } b = 0, 1, \ldots, R. \tag{5}$$

The above constitutes the simplest circumstance from an analytical perspective, and shall be referred to as being the result of receptor weighting distribution-1 (RWD-1).

Alternatively, the specific case of $\mathbf{c}(i)$ being mutually independent for $i = 1, 2, \ldots, R$ and uniformly distributed on the interval [0, 1] also allows for the direct evaluation of $P[B=b]$. We shall refer to such a possibility as RWD-2. To derive $P[B=b]$ under RWD-2, we first condition on the vector $\mathbf{v}$, and observe that consequently $B = \mathbf{c}^T \mathbf{v}$ will be a sum of independent uniform random variables. Since the components of $\mathbf{v}$ can only be 0 or 1, B will have an Irwin–Hall distribution (Johnson et al., 1995) with a probability density function (pdf) given by

$$f_{B|\mathbf{v}}(b) = \begin{cases} \frac{1}{(r-1)!} \sum_{k=0}^{\lfloor b \rfloor} (-1)^k \binom{r}{k} (b-k)^{r-1} & \text{for } r = 1, 2, \ldots, R \quad \text{and} \quad b \leq r \\ 0 & \text{otherwise} \end{cases}, \tag{6}$$

where $\lfloor . \rfloor$ denotes the floor function and, as discussed above, $r = \sum_{i=1}^{R} \mathbf{v}(i)$. It is noteworthy that in Equation (6), the case of $r = 0$ would occur only if $\mathbf{v}(i) = 0 \forall i$—which occurs with probability $(1-P)^R$—and corresponds to none of the receptors mediating an infection. In the case of $r = 0$, the infection would simply not progress any further along the axon, and the axon in question would not make a viral contribution to the ensuing stage. From Equation (6), it can be noted that it is sufficient to condition on r rather than the vector $\mathbf{v}$ (i.e., $f_{B|\mathbf{v}}(b) = f_{B|r}(b)$), accordingly the unconditioning is performed as

$$\begin{aligned} f_B(b) &= \sum_{s=1}^{R} f_{B|r=s}(b) P[r=s] \\ &= \begin{cases} \sum_{s=1}^{R} \binom{R}{s} \frac{P^s (1-P)^{R-s}}{(s-1)!} \sum_{k=0}^{\min\{\lfloor b \rfloor, \, s\}} (-1)^k \binom{s}{k} (b-k)^{s-1} & \text{for } 0 \leq b \leq R, \\ 0 & \text{otherwise} \end{cases} \end{aligned} \tag{7}$$

where we have used the fact that r has a binomial distribution. It can be noticed that Equation (7) is a mixture distribution where $\sum_{s=0}^{R} P[r=s] = 1$ with the discrete component $r = 0$ excluded from the summation in Equation (7) because it is the singular case of $B = 0$ with probability 1 since no receptors would exist. Since B is a discrete random variable we calculate its probability mass function (pmf) by discretizing the above pdf as follows:

$$\begin{aligned} P[B=b] &= \int_b^{b+1} f_B(y) dy \\ &= \sum_{s=1}^{R} \binom{R}{s} \frac{P^s (1-P)^{R-s}}{(s-1)!} \int_b^{b+1} \sum_{k=0}^{\min\{\lfloor y \rfloor, \, s\}} (-1)^k \binom{s}{k} (y-k)^{s-1} dy \qquad \text{for } b = 0, 1, \ldots, R. \end{aligned} \tag{8}$$

The above expression is studied through the simulation results shown in Figure 4. The results in Figure 4 confirm that the number of entered capsids follows a binomial distribution in the case of RWD-1. For the scenario of RWD-2, Figure 4 illustrates that the probability distributions maintain the concave shape associated with a binomial distribution. It is apparent that if binomial curves were fit to the distributions obtained for the assumption of RWD-1 and RWD-2, the former would have a noticeably higher mean. The results show a more important implication that the number of entered capsids seen with an assumption of RWD-1 may have first-order stochastic dominance (Wolfstetter, 1993) over the number of entered capsids seen with an assumption of RWD-2. This is expected since with RWD-1: $E[c(i)] = 1/2$ while with RWD-2: $E[c(i)] = 1$. In fact, a difference of factor of 2 is observed in the probability of the number of entered capsids when comparing RWD-1 and RWD-2 in Figure 4. As expected, for both RWD-1 and RWD-2, an increase in the number of receptors (R) results in an increase in the likelihood of a higher number of entered capsids. Interestingly, Figure 4 illustrates that the number of capsids is much more sensitive to P than to R. In

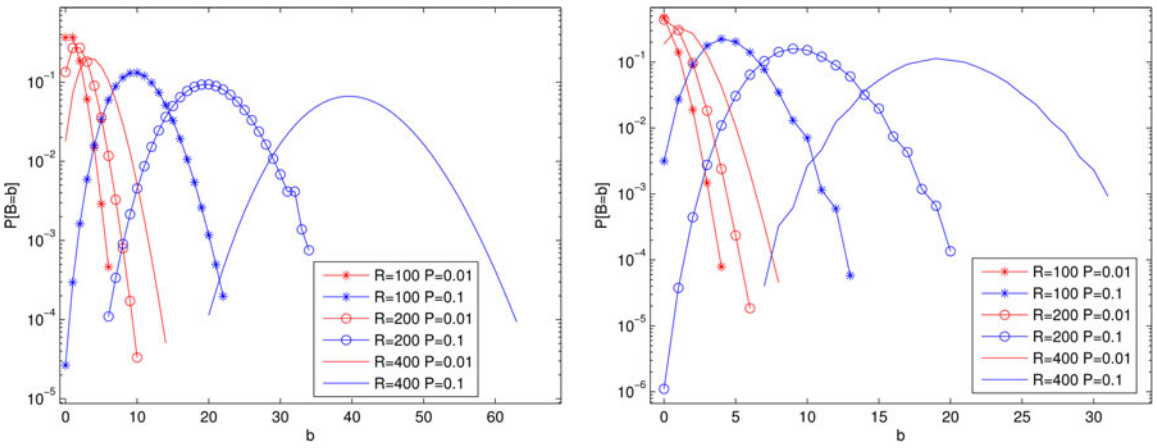

FIG. 4. Probability distribution for the number of entered capsids at the axonal invasion stage as a function of the number of receptors (R) and the probability of a receptor-mediated infection (P). The scenario of RWD-1 (left plot) is considered by computing Equation (5), whereas the scenario of RWD-2 (right plot) is evaluated by computing Equation (8) with a step size of $b_{step} = 10^{-5}$ used for the numerical integration. RWD-2, receptor weighting distribution-2.

general, there is not a global answer as to whether RWD-1 or RWD-2 is the more appropriate means of modeling the entered capsids, rather we expect that this will be dependent on the properties of the considered axon terminal.

3.3. Transport of capsids within an axon

The transport of the PRV capsids from the axon terminal shall be quantitatively modeled by the mapping of B to B' in Figure 2. The random variable B' will quantify the number of viral capsids that exhibit motion during a time period of T_1, which is typically on the order of several minutes. We assume independence and homogeneity among the viral capsids by designating P_{T_1} as the probability that each viral capsid exhibits motion during T_1 seconds. The number of active capsids B' will have a binomial distribution conditioned on the event $B=b$ leading to

$$P[B'=x|B=b]=\binom{b}{x}P_{T_1}^{x}(1-P_{T_1})^{b-x} \qquad \text{for } x=0,\,1,\,\ldots,\,b. \tag{9}$$

For the most general analysis, the probability $P[B'=x]$ may be obtained by unconditioning the above expression using Equation (4). For an assumption of RWD-1, it is possible to utilize Equation (5) to uncondition upon the event $B=b$; doing so and subsequent algebra yields the probability

$$P[B'=x]=\frac{R!}{x!}\left(\frac{P_{T_1}}{1-P_{T_1}}\right)^{x}(1-P)^{R}\sum_{b=x}^{R}\frac{1}{(b-x)!(R-b)!}\left(\frac{P(1-P_{T_1})}{1-P}\right)^{b} \qquad \text{for } x=0,\,1,\,\ldots,\,R. \tag{10}$$

Alternatively, under the assumption of RWD-2, the use of Equation (8) in conjunction with Equation (9) will result in the following probability:

$$\begin{aligned} P[B'=x] &= \sum_{b=x}^{R}\binom{b}{x}P_{T_1}^{x}(1-P_{T_1})^{b-x}P[B=b] \\ &= \sum_{b=x}^{R}\binom{b}{x}P_{T_1}^{x}(1-P_{T_1})^{b-x}\sum_{s=1}^{R}\binom{R}{s}\frac{P^{s}(1-P)^{R-s}}{(s-1)!} \\ &\quad\times\int_{b}^{b+1}\sum_{k=0}^{\min\{\lfloor b\rfloor,\,s\}}(-1)^{k}\binom{s}{k}(y-k)^{s-1}dy \qquad \text{for } x=0,\,1,\,\ldots,\,R. \end{aligned} \tag{11}$$

A quantitative study of B' is necessary since it is the variable that determines whether the PRV advances from stage 1 to the nucleus of the neuron. The simulation results of Figures 5 and 6 illustrate that, in

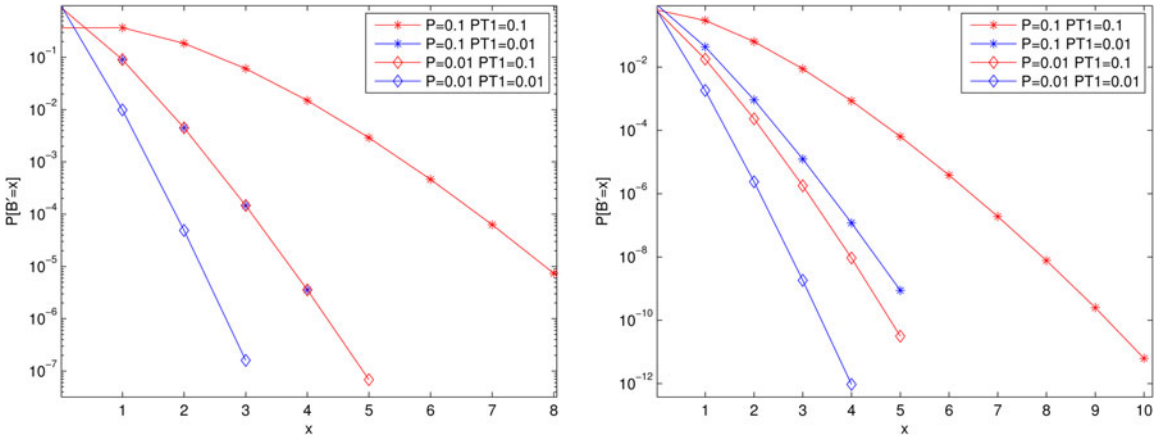

FIG. 5. Probability distribution for the number of viral capsids that exhibit motion at the axon during a time period of T_1 when the axonal invasion stage consists of $R = 100$ receptors. $P[B\prime = x]$ is computed as a function of the probability of a receptor-mediated infection (P), and the probability of a viral capsid exhibiting motion during T_1 seconds at the axonal invasion stage (P_{T_1}). The scenario of RWD-1 (left plot) is considered by computing Equation (10), whereas the scenario of RWD-2 (right plot) was evaluated by computing Equation (11).

general, the likelihood of capsids exhibiting motion during a time period of T_1 at the axonal invasion stage decreases with an increasing number of prospective capsids. For a given number of capsids, the probability of motion during the aforementioned time period generally increases with an increase in the number of receptors when comparing $R = 200$ versus $R = 100$. With respect to the impact of the RWD, the simulation results indicate that the probability of capsid motion is generally higher for RWD-1 than for RWD-2. Although Figures 5 and 6 confirm that $P[B' = x]$ decreases with decreasing values of P and P_{T_1}, it is only for the scenario of RWD-2 that P has a more pronounced affect than P_{T_1}.

3.4. Considering a multiple-axon axonal invasion stage

The number of axon terminals connected to a neuron is a variable listed in the transneuronal passage stage of Figure 1. We shall denote this variable by N and consider the case of $N = 2$ in Figure 7. For the rat

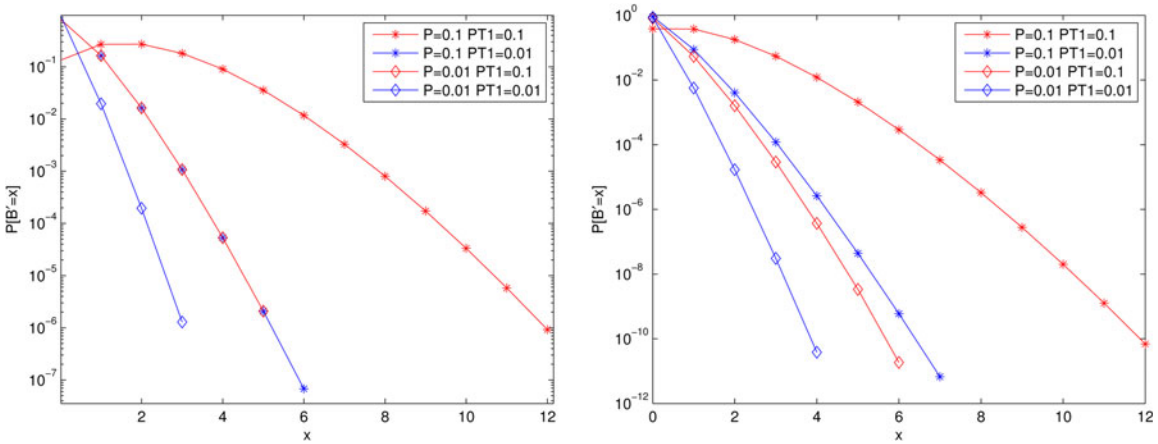

FIG. 6. Probability distribution for the number of viral capsids that exhibit motion at the axon during a time period of T_1 when the axonal invasion stage consists of $R = 200$ receptors. $P[B\prime = x]$ is computed as a function of the probability of a receptor-mediated infection (P), and the probability of a viral capsid exhibiting motion during T_1 seconds at the axonal invasion stage (P_{T_1}). The scenario of RWD-1 (left plot) is considered by computing Equation (10), whereas the scenario of RWD-2 (right plot) was evaluated by computing Equation (11).

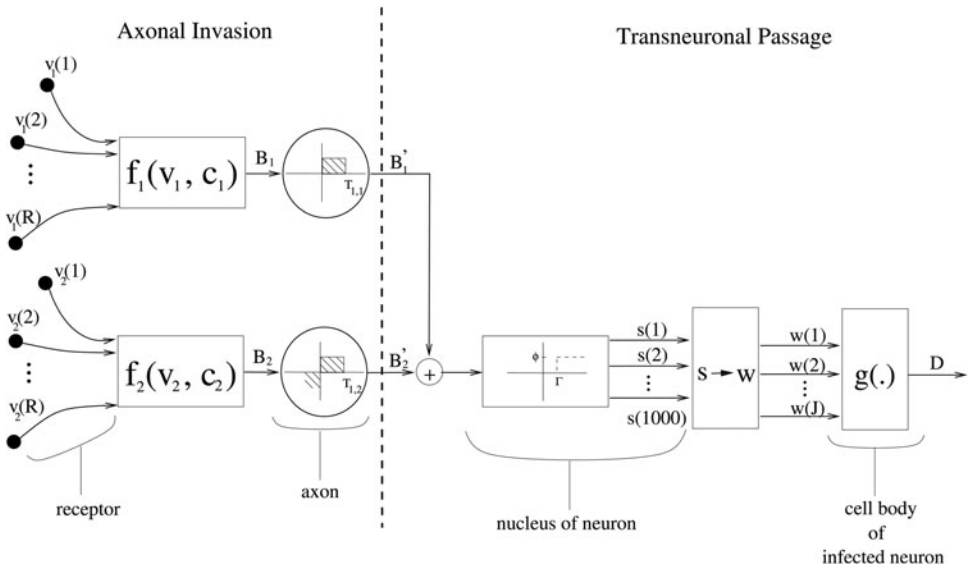

FIG. 7. An analytical model of PRV progression along the first two stages of the neural circuit consisting of a single neuron that has multiple (i.e., two) potentially infected axons.

striatum, N shall be determined by the terminal field density. Three general classes of neurons were discovered in Card et al. (1999), those that have dense, sparse, or moderate numbers of projections to the striatum. This signifies three different sets of values for N, although from a modeling perspective, the consideration of $N > 2$ shall follow readily from our analysis. The presence of two axons requires consideration of two variables B_1 and B_2 from the axonal invasion stage. Accordingly, Equation (3) is generalized to

$$B_i = f(\mathbf{v}_i, \mathbf{c}_i) = \mathbf{v}_i^T \mathbf{c}_i \qquad \text{for } i = 1, 2 \tag{12}$$

to consider the number of entered capsids from two axons. Equation (12) includes an implicit assumption that each axon is an independent unit capable of conveying an infection into the nucleus of a neuron. In the transneuronal passage stage of Figure 7, the conditional probability distributions of B'_1 and B'_2 are obtained from Equation (9). Subsequently, we initially assume that each axon will contribute equally to the progression of the infection through a summation of the form $B' = B'_1 + B'_2$.

4. STAGE 2: TRANSNEURONAL PASSAGE

The production of progeny virus is essential for the subsequent transneuronal passage of PRV between neurons. The transneuronal passage stage in Figure 1 encompasses the nucleus as well as a number of other crucial components such as the cell body. Since PRV is a DNA virus, its replication will occur in the nucleus of a neuron (Card et al., 1993). More specifically, the PRV DNA is packaged, and the capsid is assembled in the cell nucleus with the envelopment taking place in the cytoplasm. A threshold operation for the number of capsids entering the cell body of the first infected neuron shall be represented as

$$s(j) = \begin{cases} \phi & \text{for } j = 1, 2, \ldots, 1000 \quad \text{if} \quad B' > \Gamma \\ 0 & \text{for } j = 1, 2, \ldots, 1000 \quad \text{if} \quad B' \leq \Gamma \end{cases}, \tag{13}$$

where $s(j)$ denotes the virulence level of the jth particle, ϕ denotes a positive constant, and $\Gamma \in [1, 10]$ represents the minimum number of viral capsids necessary to commence viral replication in the neuron's nucleus. The probability of PRV replication is calculated according to

$$P[s(j)=\phi]=1-P[B'\leq\Gamma]=1-\sum_{x=0}^{\Gamma}P[B'=x], \tag{14}$$

where the probability of $B'=0, 1, \ldots, \Gamma$ viral capsids exhibiting motion during time period T_1 given by either Equation (10) or (11) depends on the nature of the superposition of the viral capsids at the receptors of an axon. The derivations above warrant quantitative investigation. Figure 8 examines the probability of PRV replication by computing Equation (14) for RWD-1 and RWD-2. The results implicate the Γ value as the most crucial of the considered parameters on the likelihood of virus replication. It is also noteworthy that for RWD-1, the likelihood of virus replication increases with increasing values for P or P_{T_1}, while such a relationship is not observed with RWD-2.

Replication of viral genomes and assembly of progeny virions produce an average of 1000 particles per neuron as discussed in Equation (13). A subset of those particles, J, will successfully transmit to an uninfected neuron as part of the HOI stage of viral spread. This biological process is modeled through the $\mathbf{s}\rightarrow\mathbf{w}$ transition block in the transneuronal passage stage of Figure 2. The biological implication of such operation and its resultant J-component vector $\mathbf{w}$ are discussed as follows: The $\mathbf{s}\rightarrow\mathbf{w}$ operation will map the virulence level $\phi>0$ of the viral particles into a rate λ_J for a Poisson variate. The specifics of this presumably nonlinear mapping will be determined in a future study by using experimental data from works such as Kobiler et al. (2010). Note that the virulence level ϕ will be 0 if $B'\leq\Gamma$, and in such a scenario a rate of 0 will be assigned signifying the passage of no viral particles from the cell body to the uninfected neuron.

The J particles in the cell body of the infected neuron will be modeled through a J-dimensional vector $\mathbf{w}$, with J having a Poisson distribution with rate λ_J. It shall be assumed that $\lambda_J\gg1000$, and thus $P[J<1000]\approx1$. In Kobiler et al. (2010), it was discovered that the average number of viral genomes that are expressed or replicated per cell (i.e., $E[J]$) lies between four and seven irrespective of the multiplicity of infection. Although the finding was for non-neuronal cells, the same authors have recently shown that the result also holds for neurons (Taylor et al., 2012). From Figure 5 of Kobiler et al. (2010), we posit that $E[J]=\lambda_J=5$. The $1000-J$ particles that do not proceed from the infected neuron are referred to as defective particles (McLauchlan and Rixon, 1992; Szildgyi and Berriman, 1994). Defective particles are incapable of propagating infection, and are either removed by phagocytic microglia and macrophages, or spread to another cell such as an astrocyte. The two possibilities are analytically identical, because in both cases the defective particles will not affect the progression of the PRV through the circuit. At this point, we shall have

$$P[J=j\,|\,B'>\Gamma]=\begin{cases}\lambda_J^j\exp(-\lambda_J)/j! & j=0,1,2,\ldots\\ 0 & \text{otherwise}\end{cases}, \tag{15}$$

where $\lambda_J=5$; the above probability shall be referred to as $P[J=j\,|\,\text{FOI}]$ to highlight the fact that the quantity is contingent on the occurrence of a first-order infection (FOI).

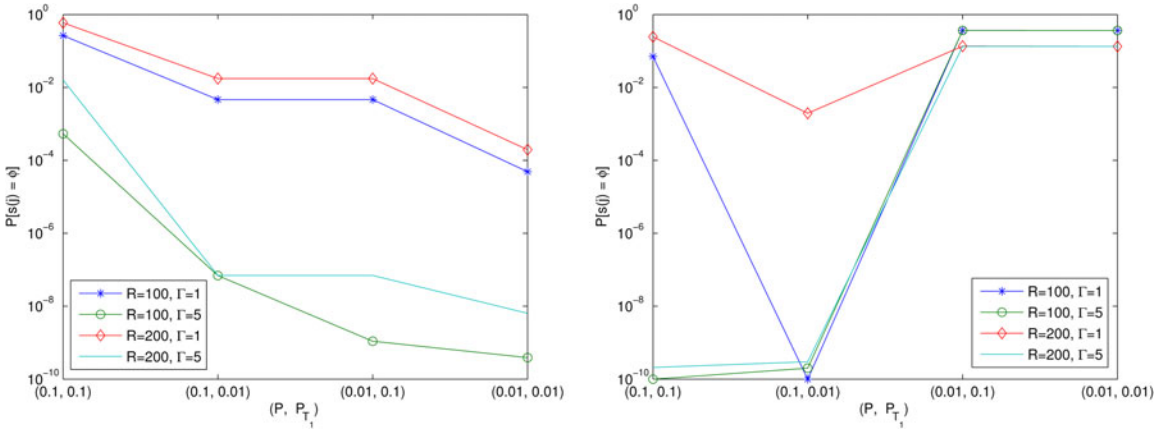

FIG. 8. The probability of PRV replication is computed through Equation (14). The scenario of RWD-1 (left plot) was considered by using the B' values obtained from Equation (10), whereas the scenario of RWD-2 (right plot) was considered by using the B' values obtained from Equation (11).

In Figure 2, the function $g(\cdot)$ shall model an operation on the J particles before the entrance of the virus into an axon of a downstream neuron, and the metric D will quantify the number of capsids entering an axon. We restrict the function $g(.)$ to a linear summation through $D = g(\mathbf{w}, \mathbf{h}) = \mathbf{w}^T\mathbf{h}$ by introducing the vector $\mathbf{h} \in \mathbb{R}^J$, which contains weights that will model the superposition of the particles at the cell body of the infected neuron. Recent empirical evidence from works such as Taylor et al. (2012) indicates that the J particles are identical. Hence, we shall consider a scenario of the particles being identical and weighted equally in the combining operation through the assignment $\mathbf{h} = \mathbf{w} = [1, 1, \ldots, 1]$. Consequently, the number of capsids entering the axon will be determined through a counting operation as

$$D = g(\mathbf{w}, \mathbf{h}) = \mathbf{w}^T\mathbf{h} = J. \tag{16}$$

The above analysis serves as a sensible initial account for a rather complex process, and will lead to $P[J = j|\text{FOI}] = P[D = j|\text{FOI}]$, with the latter denoting the probability distribution for the number of capsids entering an axon for a prospective HOI.

4.1. Considering a multiple-neuron transneuronal passage stage

To present a realistic view of the virus progression along a neural circuit, multiple neurons will need to be considered. This section contains analysis corresponding to Figure 9, which considers the transneuronal passage stage of the neural circuit being comprised of multiple neurons. The inputs to the transneuronal passage stage in Figure 9 maintain the same structure as that introduced in Figure 7 with the contributions from various axons summing together to provide an aggregate number of active capsids. The output of the transneuronal passage stage will be a sequence $D_1, D_2, \ldots, D_q$, with q denoting the number of neurons in the transneuronal passage stage that project to downstream neurons to beget a HOI. Subsequently, each of the q outputs would be processed by a HOI stage whose operation shall be discussed in Section 5, Stage 3: HOI.

5. STAGE 3: HOI

The progression of PRV infection in a neural circuit involves virion transmission to synaptically connected cells, which leads to a HOI. The analysis and quantification of such a progression will be presented

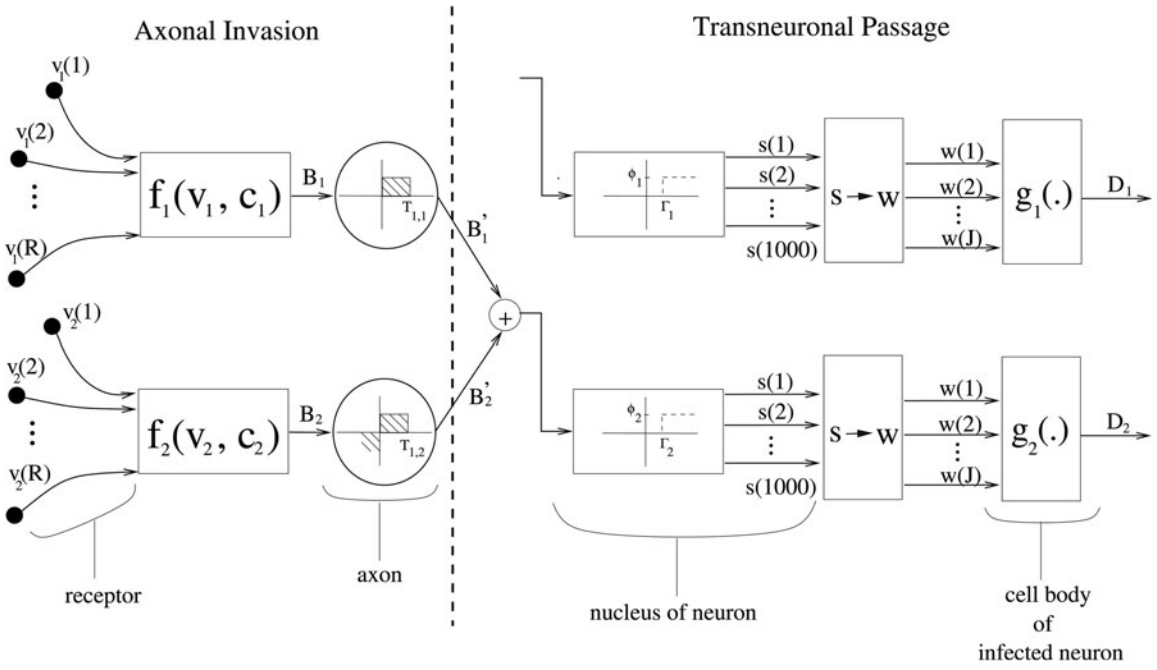

FIG. 9. A model for PRV progression along the first two stages of the neural circuit with multiple neurons. The above depicts two neurons with the second neuron containing two potentially infected presynaptic axons.

in the final stage of the model motivated by Figure 1. The infection of ancillary cells such as astrocytes that do not form synaptic connections to other cells will not be deemed relevant within the context of determining an infection or the spread of PRV. Figure 3 depicts a model for the SOI stage shown in Figure 1. In Figure 3, the metric D' represents the number of capsids that exhibit motion during a time period of T_2. Such capsids would have stemmed from the D capsids that entered the cell body of an infected neuron at a prior transneuronal stage. The derivation of the statistical properties of D' is similar to the analysis for B' in Section 3.3. Namely, the number of active capsids will have a binomial distribution conditioned on the event $D=y$ through

$$P[D'=x|D=y]=\binom{y}{x}P_{T_2}^{x}(1-P_{T_2})^{y-x} \qquad \text{for } x=0,\,1,\,\ldots,\,y, \tag{17}$$

where y is a positive integer. At the nucleus of the second-order neuron, a threshold operation similar to the operation in the nucleus of the primary neuron is modeled through

$$s(j)=\begin{cases}\phi & \text{for } j=1,\,2,\,\ldots,\,1000 \quad \text{if} \quad D'>\Gamma_2\\ 0 & \text{for } j=1,\,2,\,\ldots,\,1000 \quad \text{if} \quad D'\le\Gamma_2\end{cases}, \tag{18}$$

where $\Gamma_2 \in [1, 10]$ represents the minimum number of viral capsids necessary to commence viral replication. The probability of PRV replication in the second-order neuron's nucleus is calculated according to

$$\begin{aligned}P[s(j)=\phi]&=1-P[D'\le\Gamma_2]=1-\sum_{x=0}^{\Gamma_2}P[D'=x]\\&=1-\sum_{x=0}^{\Gamma_2}\left(\sum_{y=x}^{\infty}P[D'=x|D=y]P[D=y]\right)\\&=1-\sum_{x=0}^{\Gamma_2}\left(\sum_{y=x}^{\infty}\binom{y}{x}P_{T_2}^{x}(1-P_{T_2})^{y-x}\lambda_J^{y}\exp(-\lambda_J)/y!\right).\end{aligned} \tag{19}$$

In the above expression, the probability $P[D=y|\text{FOI}]$ given by Equation (15) is used in place of $P[D=y]$ because a SOI can only be considered if a FOI has occurred. The probability of a SOI is thus expressed as

$$P[\text{SOI}]=(1-P[B'\le\Gamma])(1-P[D'\le\Gamma_2]), \tag{20}$$

where the above expression contains the constituent probabilities provided by Equations (19) and (14). The above expression unifies the analysis undertaken for the three-stage model and provides a concise means to estimate the likelihood of a SOI. We consider the axons synapsing onto a neuron as the only location where virus particles can propagate from an infected presynaptic neuron to an uninfected postsynaptic neuron.

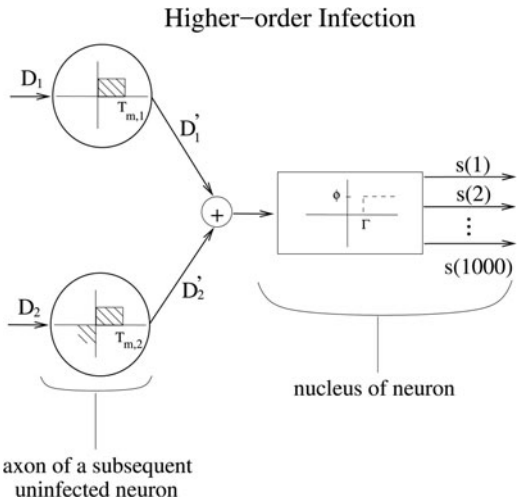

FIG. 10. A depiction of PRV progression along the HOI stage of the neural circuit. One $m+1$th-order neuron is shown with two axons connecting it to the transneuronal passage stage of what could be either a single or two distinct mth-order infected neurons.

Accordingly, the case of multiple infected axons conveying the infection to an uninfected neuron would be modeled through the superposition $D' = D_1{}' + D_2{}'$. This is modeled through the HOI stage shown in Figure 10. Computing the probability of HOI beyond the second order would encompass repeating the functionality presented in Figure 3 for each subsequent stage of downstream neurons. For instance, the probability of a third-order infection would be expressed as

$$\begin{aligned} P[\text{TOI}] &= (1 - P[B' \leq \Gamma])(1 - P[D' \leq \Gamma_2])P[s(j) = \phi] \\ &= (1 - P[B' \leq \Gamma])(1 - P[D' \leq \Gamma_2])(1 - P[D'' \leq \Gamma_3]) \\ &= P[\text{SOI}](1 - P[D'' \leq \Gamma_3]). \end{aligned} \tag{21}$$

It should be evident that the progression of a HOI along the neural circuit is governed by a Markov process, more specifically a birth process. The above expression presents a recursive relationship for evaluating the HOI probabilities, with each HOI stage being characterized by a λ_J, T, P_T, and Γ value.

PRV particles are frequently referred to as self-amplifying in the sense that when a particle replicates in the cell nucleus, it results in the multiplicative affect of begetting ~ 1000 particles. The presented model accounts for this effect in the transneuronal passage and HOI stages. In addition, PRV is often referred to as a sparse labeler because not all of the neurons in a neural circuit are ultimately labeled by this tracer. The sparsity occurs because of several limiting factors: First, at the initial site of infection a limited number of axon terminals take up the virus. Since there is an estimate of only 1000 particles per neuron, and there may be 10,000 synapses per neuron, it may be impossible to infect all synapses. The second limiting factor is the all-or-nothing thresholding operation in the nucleus of the higher order neuron. A third limiting factor is antiviral response, namely interferon signaling has been shown to prevent more extensive spread from sites of primary replication (Mikloska and Cunningham, 2001; Rosato and Leib, 2015).

6. CONCLUSIONS AND FUTURE WORK

This work proposes a three-stage architecture to analytically model the progression of PRV Bartha from the axonal invasion stage to transneuronal passage and a HOI. Our analysis commenced by translating a diagram for the ingress of PRV through a peripheral or intracerebral injection and the retrograde transport to neurons into a three-stage schematic. The subsequent computational analyses have been based on operations posited to occur according to the virology literature. At each stage of the model, several parameters and quantitative operations were identified as being important in the behavior of the virus progression. The proposed operations are subject to change as additional experiments are performed yielding new datasets. As more empirical data become available, increasingly precise numerical values for the variables discussed in Table 1 can be incorporated into the presented model to predict the probability of HOI and spread of the injected PRV.

A second objective of the modeling is to identify parameters whose numerical values should be determined by virologist through future experimentation. Efforts to quantitatively model the progression of the injected viral tracer in neural circuits remain absent from the literature. Quantitative methods for estimating the likelihood of the virus replicating at a primary neuron and the probability of a HOI in a neural circuit should complement empirical research. In stage 1, modeling receptor engagement and uptake of injected virus identified an absence of information related to receptor density and accessibility. In stage 2, modeling the establishment and progression of infection within the primary neuron identified the necessity of having information about how frequently viral infection does not elicit productive viral replication. Similarly, for stage 3 the modeling of SOI and HOI required knowledge of progeny virion competency. Similar to the scenario with stage 2, it is not known how often a viral particle is not capable of propagating infection. The only means to attain values for such variables is through experimental methods that provide empirical assessments on different aspects of viral spread in the nervous system.

While limited, various research groups have attempted to quantify the transmission of herpesviruses [reviewed in Herr et al. (2017)]. A great deal of work has analyzed the efficiency of viral particle transport in the nervous system. Two studies have even quantified the timing and efficiency of viral particle transport in in vivo neuronal infections (LaVail et al., 2003; Granstedt et al., 2013). Similarly, extensive work has quantified the capacity of cells to be coinfected by multiple herpesviruses. By

Table 1. A Litany of the Parameters Discussed in the Presented Model

Parameter	*Representative values*	*Description*
α_i	TBD	Contribution of the proximity of the receptor to the point of injection in determining a receptor-mediated infection.
β_i	TBD	Contribution of the affinity of the axon terminal to a receptor-mediated infection.
γ_i	TBD	Contribution of the affinity of glia to a receptor-mediated infection.
ω_i	TBD	Contribution of the affinity of extracellular matrix to determining a receptor-mediated infection.
W	[0, 1]	Anatomical indication of the likelihood of infection.
d_i	(0, 1500] μm	Distance from the ith receptor to the point of injection at the axonal invasion stage.
$\bar{d}$	(0, 1500] μm	Mean receptor distance to the point of injection for the close vicinity surrounding the injection area.
T_1	A few seconds	Considered time window over which viral capsids exhibit motion after entering the axon of a primary neuron.
T_2	$>$ 10 hours	Considered time window over which viral capsids exhibit motion after proceeding from an infected primary neuron to a subsequent (i.e., second-order) neuron.
P_{T_i}	[0,1]	$i=1$: probability of a viral capsid exhibiting motion during T_1 seconds at the axonal invasion stage. $i=2$: probability of a viral capsid exhibiting motion during T_2 seconds at the axonal invasion stage of a second-order neuron.
Γ	[1, 10]	The minimum number of viral capsids necessary to commence the replication of an infection in a neuron's nucleus.
$E[J]$	[4,7]	The mean number of viral genomes that are expressed or replicated per cell.
R	$\gg 1$	Number of receptors entering an axon.
$P[R_i=I]$	[0,1]	Probability of receptor-mediated infection at the axonal invasion stage.
$f(\mathbf{x}, \mathbf{y})$	$\mathbf{x}^T\mathbf{y}$	Operation performed by the axonal invasion stage on the receptor outputs to determine the number of entered capsids.
$g(\mathbf{x}, \mathbf{y})$	$\mathbf{x}^T\mathbf{y}$	Operation performed at the cell body of an infected neuron on the J particles entering the cell body in arriving at the number of viral capsids that enter the axon of a downstream neuron.

The represented values have been determined from rat striatum data reported in Card et al. (1999), and the operations $f(\cdot, \cdot)$ and $g(\cdot, \cdot)$ were posited as an initial account. The range of T_1 and T_2 values was gathered from Granstedt et al. (2013) and Antinone and Smith (2010). Values for several of the introduced parameters are currently unknown and warrant empirical measurement TBD.

TBD: to be determined.

studying the distribution of fluorescent protein expressing viruses, Kobiler et al. (2010) found that a maximal level of coinfection, approximating eight viral genomes, can be supported by infected cells. Further, the distribution of fluorescent protein coexpression could be modeled as a Poisson-based distribution of viral replication. Works such as Kobiler et al. (2010) have considered parametric estimation of a parameter discussed in our model by assuming a Poisson distribution and finding maximum-likelihood (ML) estimates of the average number of viral genomes expressed per cell (i.e., $E[J]$). Unfortunately, ML estimation cannot be applied when virtually nothing is known (or presumed) about the underlying distribution. This presents a challenge from the statistical point of view, and the utility of methods such as Geman and Hwang (1982) should be investigated.

In fact, decisions must be made as whether to consider a nonparametric technique, or to speculate probability distributions for the parameters without much a priori information and then derive ML estimates. The second alternative, while probably simpler, has the drawback of fitting to an underlying distribution that may not be completely accurate in representing the virology. The studies mentioned above have already been implemented in in vitro models of viral spread (Taylor et al., 2012), identifying potential restrictions to second-order coinfection that can inform the mathematical models detailed in stages 2 and 3. In fact, work in progress has extended these coinfection experiments to map the neurotropic spread within an in vivo circuit (Herr and Thornburg, 2018). While the information derived from the aforementioned studies cannot define the variables needed to refine the mathematical models, they do provide insight into future experimental designs. Such experiments will be challenging to conduct; therefore, it is important to have justifying rationale behind their significance.

ACKNOWLEDGMENTS

The authors thank Lynn Enquist and J. Patrick Card for introducing them to the problem statement, and providing very helpful discussions on the translation of biology into the model.

AUTHOR DISCLOSURE STATEMENT

The authors declare that no competing financial interests exist.

REFERENCES

Antinone, A., and Smith, G.A. 2010. Retrograde axon transport of herpes simplex virus and pseudorabies virus: A live-cell comparative analysis. *J. Virol.* 84, 1504–1512.

Cano, G., Card, J.P., and Sved, A. 2004. Dual viral transneuronal tracing of central autonomic circuits involved in the innervation of the two kidneys in rat. *J. Comp. Neurol.* 471, 462–481.

Cano, G., Sved, A., Rinaman, L., et al. 2001. Characterization of the CNS innervation of the rat spleen using viral transneuronal tracing. *J. Comp. Neurol.* 439, 1–18.

Card, J.P., and Enquist, L.W. 2012. Use and visualization of neuroanatomical viral transneuronal tracers, 225–268. *In* Badoer, E., eds. *Visualization Techniques: From Immunohistochemistry to Magnetic Resonance Imaging*, Vol 70. Totowa, NJ: Humana Press.

Card, J.P., Enquist, L.W., and Moore, R.Y. 1999. Neuroinvasiveness of pseudorabies virus injected intracerebrally is dependent on viral concentration and terminal field density. *J. Comp. Neurol.* 407, 438–452.

Card, J.P., Rinaman, L., Lynn, R.B., et al. 1993. Pseudorabies virus infection of the rat central nervous system: Ultrastructural characterization of viral replication, transport, and pathogenesis. *J. Neurosci.* 13, 2515–2539.

Enquist, L.W. 2012. Five questions about viral trafficking in neurons. *PLoS Pathog*. 8, e1002472.

Geman, S., and Hwang, C.R. 1982. Nonparametric maximum likelihood estimation by the method of sieves. *Ann. Stat.* 10, 401–414.

Granstedt, A., Brunton, B., and Enquist, L.W. 2013. Imaging the transport dynamics of single alphaherpesvirus particles in intact peripheral nervous system explants from infected mice. *mBio.* 4, 1–13.

Herr, A.E., Hain, K.S., and Taylor, M.P. 2017. Limitations on the multiplicity of cellular infection during human alphaherpesvirus disease. *Curr. Clin. Microbiol. Rep.* 4, 167–174.

Herr, A.E., Thornburg, T., et al. 2018. The route of transmission impacts pseudorabies virus coinfection in vivo. In preparation for submission.

Jasmin, L., Burkey, A.R., Card, J.P., et al. 1997. Transneuronal labeling of a nociceptive pathway, the spino-(trigemino-)parabrachio-amygdaloid, in the rat. *J. Neurosci.* 17, 3751–3765.

Johnson N, Kotz, S., and Balakrishnan, N. 1995. *Continuous Univariate Distributions*. Wiley, New York, NY.

Kobiler, O., Lipman, Y., Therkelsen, K., et al. 2010. Herpesviruses carrying a Brainbow cassette reveal replication and expression of limited numbers of incoming genomes. *Nat. Commun*. 1, 146.

LaVail, J.H., Tauscher, A.N., Aghaian, E., et al. 2003. Axonal transport and sorting of herpes simplex virus components in a mature mouse visual system. *J. Virol.* 77, 6117–6126.

McLauchlan, J., and Rixon, F. 1992. Characterization of enveloped tegument structures (L particles) produced by alphaherpesviruses: Integrity of the tegument does not depend on the presence of capsid or envelope. *J. Gen. Virol.* 73, 269–276.

Mikloska Z., and Cunningham A., 2001. Alpha and gamma interferons inhibit herpes simplex virus type 1 infection and spread in epidermal cells after axonal transmission. *J. Virol*. 75, 11821–11826.

Pomeranz, L.E., Reynolds, A.E., and Hengartner, C.J. 2005. Molecular biology of pseudorabies virus: Impact on neurovirology and veterinary medicine. *Microbiol. Mol. Biol. Rev.* 69, 462–500.

Rosato, P., and Leib, D. 2015. Neuronal interferon signaling is required for protection against herpes simplex virus replication and pathogenesis. *PLoS Pathog*. 11, e1005028.

Spear, P.G. 1993. Entry of alphaherpesviruses into cells. *Semin. Virol.* 4, 167–180.

Szildgyi, J., and Berriman J. 1994. Use and visualization of neuroanatomical viral transneuronal tracers. *J. Gen. Virol.* 75, 1749–1753.

Takai, Y., and Nakanishi, H. 2003. Nectin and afadin: Novel organizers of intercellular junctions. *J. Cell Sci*. 116, 17–27.

Taylor, M.P., Kobiler, O., and Enquist, L.W. 2012. Alphaherpesvirus axon-to-cell spread involves limited virion transmission. *Proc. Natl. Acad. Sci. USA*. 407, 17046–17051.

Trybala, E., Bergström, T., Spillmann, D., et al. 1998. Interaction between pseudorabies virus and heparin/heparan sulfate. Pseudorabies virus mutants differ in their interaction with heparin/heparan sulfate when altered for specific glycoprotein C heparin-binding domain. *J. Biol. Chem.* 273, 5047–5052.

Wolfstetter, E. 1993. Stochastic dominance: Theory and applications. Humboldt-Univ., Wirtschaftswiss. Fak. at Berlin.

Address correspondence to:
Mr. Siamak K. Sorooshyari
Johnson & Johnson
Bridgewater, NJ 08807

E-mail: siamak.sorooshyari@gmail.com